BMC Medicine

RESEARCH

Open Access

Normative structural connectome constrains spreading transient brain activity in generalized epilepsy

Jie Xia[1,2], Siqi Yang[3], Jiao Li[1,2], Yao Meng[1,2], Jinpeng Niu[1,2], Huafu Chen[1,2], Zhiqiang Zhang[4] and Wei Liao[1,2*]

Abstract

Background Genetic generalized epilepsy is characterized by transient episodes of spontaneous abnormal neural activity in anatomically distributed brain regions that ultimately propagate to wider areas. However, the connectome-based mechanisms shaping these abnormalities remain largely unknown. We aimed to investigate how the normative structural connectome constrains abnormal brain activity spread in genetic generalized epilepsy with generalized tonic–clonic seizure (GGE-GTCS).

Methods Abnormal transient activity patterns between individuals with GGE-GTCS ($n=97$) and healthy controls ($n=141$) were estimated from the amplitude of low-frequency fluctuations measured by resting-state functional MRI. The normative structural connectome was derived from diffusion-weighted images acquired in an independent cohort of healthy adults ($n=326$). Structural neighborhood analysis was applied to assess the degree of constraints between activity vulnerability and structural connectome. Dominance analysis was used to determine the potential molecular underpinnings of these constraints. Furthermore, a network-based diffusion model was utilized to simulate the spread of pathology and identify potential disease epicenters.

Results Brain activity abnormalities among patients with GGE-GTCS were primarily located in the temporal, cingulate, prefrontal, and parietal cortices. The collective abnormality of structurally connected neighbors significantly predicted regional activity abnormality, indicating that white matter network architecture constrains aberrant activity patterns. Molecular fingerprints, particularly laminar differentiation and neurotransmitter receptor profiles, constituted key predictors of these connectome-constrained activity abnormalities. Network-based diffusion modeling effectively replicated transient pathological activity spreading patterns, identifying the limbic-temporal, dorsolateral prefrontal, and occipital cortices as putative disease epicenters. These results were robust across different clinical factors and individual patients.

Conclusions Our findings suggest that the structural connectome shapes the spatial patterning of brain activity abnormalities, advancing our understanding of the network-level mechanisms underlying vulnerability to abnormal brain activity onset and propagation in GGE-GTCS.

Keywords Disease epicenter, Generalized epilepsy, Network spreading, Structural connectome, Transient brain activity

*Correspondence:
Wei Liao
weiliao.wl@gmail.com
Full list of author information is available at the end of the article

Background

Genetic generalized epilepsy with generalized tonic–clonic seizure (GGE-GTCS) is a seizure disorder typically characterized by bilateral spike-wave discharges that spread from anatomically distributed regions to disrupt large-scale brain networks [1, 2]. The amplitude of low-frequency fluctuation (ALFF) on functional magnetic resonance imaging (fMRI) is a particularly sensitive metric for localizing spontaneous activity [3]. While the spatial distribution of ALFF abnormalities is heterogeneous among GGE-GTCS patients, the most pronounced usually appear in the posterior cingulate cortex, prefrontal lobe, and temporal lobe [4–6]. Despite numerous studies describing the location and nature of these brain activity anomalies [4–6], the network-level mechanisms shaping their characteristic spatial pattern remain unclear.

The human brain is composed of multiple, interconnected, hierarchically organized networks, and understanding how these networks interact at a brain-wide level has proven crucial for elucidating the pathogenesis of brain diseases [7, 8]. The complex connectome architecture fundamentally shapes brain disorder occurrence, manifestations, and progression [9, 10]. Thus, anatomical connections likely serve as conduits for propagating pathological and physiological events. The connectome enables pathogenic processes, such as neuronal activity, to spread from lesions or epicenters to other regions, disrupting global information processing [11, 12]. Recently, network neighborhood analysis [13] was proposed to predict regional abnormality based on mean abnormalities in topologically connected neighborhoods, and successfully applied to neurodegenerative and psychiatric disease research [13–16]. These studies support the hypothesis that the spread of brain dysfunction reflects underlying network architecture. The spatial patterning of ALFF alterations in GGE-GTCS is anchored to specific networks [4, 5], raising the possibility that connectome architecture constrains and shapes the spread of GGE-GTCS pathology.

Network-based diffusion models have contributed immensely to a deeper mechanistic understanding of pathological propagation in brain disease [17–19]. These models simulate the interregional diffusive spread of pathology by utilizing topological information from the structural connectome [20, 21]. For instance, a diffusion mechanism mediated through brain networks can effectively recapitulate the spread of gray matter atrophy in neurodegenerative conditions [22, 23]. Network-based spreading processes may also be involved in generalized epilepsy. Recent studies have applied network-based atrophy modeling to identify disease epicenters in generalized epilepsy [8, 14], suggesting that specific epicenters' connectivity profiles constrain the pathophysiology's spread. Disease epicenter mapping can identify regions whose connectivity profiles closely resemble syndrome-specific dysfunction patterns [8]. The application of such models to generalized epilepsy is justified because the syndrome is related to brain network pathology [24, 25]. Therefore, network-based modeling may elucidate how abnormal neural activity spreads from disease epicenters into connected brain regions, providing an innovative approach to test hypotheses regarding vulnerability to the spread of pathological brain activity in GGE-GTCS.

In the current study, utilizing neuroimaging, connectome, molecular fingerprints, and network-based computational models, we tested the hypothesis that the normative structural connectome constrains the spread of transient brain activity anomalies in GGE-GTCS by (i) mapping distributed ALFF alteration patterns in patients, (ii) assessing the degree of constraints between regional ALFF abnormality and its structurally connected neighbors, (iii) quantifying the contribution of molecular profiles to connectome-constrained ALFF abnormalities, and (iv) utilizing a network-based diffusion model to simulate the spread of transient activity and identify potential disease epicenters.

Methods

Participants

All study procedures were conducted according to the Helsinki Declaration of 1975 and approved by the medical ethics committee of Jinling Hospital, School of Medicine, Nanjing University, China (approval number: 2014GJJ-056). Written informed consent was obtained from all participants.

All patients were diagnosed as GGE with only GTCS by two experienced neurologists following the International League Against Epilepsy (ILAE) criteria [1]. Patient inclusion criteria were as follows: (1) typical clinical symptoms of GTCS, including limb twitching and loss of consciousness, without preceding symptoms of partial seizures; (2) presence of generalized spike-and-wave discharges on electroencephalogram (EEG); (3) no apparent etiology history, and (4) no remarkable abnormalities on structural MRI. Moreover, patients were excluded if they had (1) progressive diseases, tumors, or previous neurosurgery, (2) incomplete MRI scanning results, or (3) head motion exceeding 3 mm or 3°. Eventually, the study included 97 patients with GGE-GTCS ($n = 97$; 32 females; age = 24.89 ± 7.71 years) who met patient inclusion and exclusion criteria.

Antiseizure medications (ASMs) are a significant cause of sudden unexpected death in epilepsy [26]. Medication information was not available for six patients. The mean number of ASMs per patient was 1.03, ranging from 0 to 4 ASMs. Specifically, twenty-eight patients were not

on any medication, forty were on monotherapy, and the remaining patients had polytherapy. Additionally, the patients did not undergo neuropsychological assessment [27–29].

A demographically matched cohort of healthy controls (HCs) ($n=141$; 62 females; age = 27.47 ± 6.34 years) was included. Healthy participants had no history of neurological or psychiatric disorders. The detailed demographic and clinical characteristics are summarized in Additional file 1: Table S1. There were no significant differences in sex, age, and handedness ratio between groups (all $P>0.05$).

Data acquisition and preprocessing

Structural and functional images were acquired on a Siemens Trio 3 T scanner (Siemens, Munich, Germany) at Jinling Hospital. We employed foam padding to reduce head motion. All participants were required to keep their eyes closed, keep their heads still, and avoid falling asleep. Resting-state fMRI data were obtained using an echo planar imaging (EPI) sequence (repetition time (TR) = 2000 ms, echo time (TE) = 30 ms, flip angle = 90°, field of view (FOV) = 240 × 240 mm^2, matrix size = 64 × 64, 30 transverse slices, slice thickness = 4 mm, and interslice gap = 0.4 mm) aligned along the anterior commissure-posterior commissure line. Each participant was scanned with a total of 250 volumes. The total scan time was 500 s. Subsequently, the T1-weighted (T1w) images were acquired using a magnetization-prepared rapid gradient echo sequence (TR = 2300 ms, TE = 2.98 ms, flip angle = 9°, FOV = 256 × 256 mm^2, matrix size = 256 × 256, slice thickness = 1 mm, and slices = 176).

The T1w images were preprocessed using the FreeSurfer pipeline (v6.0.1, https://surfer.nmr.mgh.harvard.edu/) [30], which includes skull-stripping, tissue segmentation, and surface reconstruction. Functional data were preprocessed following the Computational Brain Imaging Group (CBIG) pipeline (v1.5.1, https://github.com/ThomasYeoLab/CBIG.) as in previous studies [31–33]. Steps included exclusion of the initial four volumes, slice timing, and motion correction, followed by co-registration to the T1w images. Frame-wise displacement (FD) was computed using the FSL toolbox. Time frames exhibiting FD > 0.5 mm and neighboring time frames were identified as outliers and interpolated using the least-square interpolation of neighboring time frames. Participants with a mean FD (mFD) exceeding 0.5 mm were excluded from the analysis. To further control for noise and motion effects, 18 nuisance regressors were regressed, including the six head-motion estimates, the white matter signal, the ventricular signal, the global brain signal, and their temporal derivatives [31]. All preprocessed time courses were band-pass filtered at 0.01–0.08 Hz to eliminate noise effects. Finally, denoised functional signals were resampled into a standard"fsaverage6"space and smoothed with a 6-mm full-width at half-maximum of Gaussian kernel.

Normative structural connectome

Diffusion-weighted imaging (DWI) data were obtained from 326 unrelated healthy adults ($n=326$; 181 females; age: 22–35 years) of the Human Connectome Project [34]. DWI data were acquired on a Siemens Skyra 3 T scanner using a spin-echo EPI sequence with the following parameters [34]: TR = 5520 ms, TE = 89.5 ms, FOV = 210 × 180 mm^2, voxel size = 1.25 mm^3, b-values = 1000, 2000, and 3000 s/mm^2, 270 diffusion directions, and 18 b0 images.

DWI data were preprocessed via the MRtrix3 software (v3, https://www.mrtrix.org/) [35]. Briefly, fiber orientation distributions were generated using a constrained spherical deconvolution algorithm. Probabilistic streamline tractography was applied to reconstruct white matter streamlines. Then, spherical-deconvolution-informed filtering of tractograms (SIFT2) was utilized to optimize the streamlines. The reconstructed streamlines were projected onto the Schaefer-400 atlas [36] to generate individual structural connectivity. Finally, the group consensus normative structural connectome (SC) was constructed to preserve the density and edge length distribution across participants [37]. The weights of edges in a group-level network were defined by the logarithmic transformation of non-zero streamline counts.

Fluctuation amplitude quantification

To estimate fluctuation amplitude, we first transformed the preprocessed surface-based fMRI time series from the time domain to the frequency domain, and generated the power spectrum within the 0.01 to 0.08 Hz range. The average square root of the power spectrum was then calculated as the ALFF [3]. Surface-based brain activity was used to measure ALFF, ensuring more precise cross-subject matching of functional anatomy [4, 38]. Finally, the vertex-wise ALFF was parcellated into 400 cortical areas using the Schaefer-400 atlas [36] to acquire the mean ALFF value within individual regions.

Case–control analysis of regional ALFF

A general linear model was constructed to estimate regional ALFF abnormalities between patient and HC groups, with regional ALFF values as the dependent variable, sex, age, and head motion (mFD) as regression covariates, and group as the main effect. This model was constructed to fit each cortical region and generate t-values and P-statistics to represent between-group differences. The significance threshold was set at $P<0.05$

with false-discovery rate (FDR) correction across 400 regions. We applied unthresholded *t*-values as inputs for our models, enabling us to model the spatial pattern of ALFF abnormalities across the entire brain, rather than only differences that survived a statistical threshold.

To test whether the spatial patterning of ALFF abnormalities was anchored to specific brain systems, we first divided cortical regions into intrinsic functional networks defined by the Yeo atlas [39] and laminar differentiation classes based on the Mesulam atlas [40]. We then calculated the mean ALFF difference values within each network and compared the empirical values to a null distribution of mean difference magnitudes generated through a spatial permutation test (spin test) (see Additional file 1: Method S1 for details) [41, 42]. Significance was set at $P_{spin} < 0.05$ with false discovery rate (FDR)-correction for multiple comparisons. The mean *t*-values of each system were converted to z-scores relative to this null distribution. A positive z-score represents a greater difference than expected, and vice versa.

Structural neighborhood analysis

We evaluated the relationships between regional ALFF abnormality (*t*-value between GGE-GTCS and HC groups) and its directly structurally connected neighbor to test whether structural connectome constrains ALFF abnormalities. Briefly, the collective abnormality of structural neighbors of region *i* was quantized as the average abnormality of all regions that were connected to region *i* by a structural connectome (see Additional file 1: Method S2 for details) [13]. We then assessed the spatial correlation between empirical ALFF abnormalities (*t*-values) and collective ALFF abnormality values using Pearson's correlation coefficients. Finally, we assessed the variation in spatial constraint at the system level by examining if the constraint was stronger in specific intrinsic functional networks [39] and laminar differentiation classes [40].

Molecular fingerprints underpinning SC-constrained activity abnormalities

If the structural connectome constrains ALFF abnormalities, it is essential to clarify whether this constraint is associated with molecular attributes. We constructed a multilinear regression model with four molecular predictors to illustrate the molecular contributions to the constraints of ALFF abnormalities by SC.

Gene expression gradient

The principal axis of disease-specific gene expression profiles (gene PC1) represents a hierarchical gradient of transcriptomic specialization [43], which reflects disease pathophysiology associated with generalized epilepsy. Microarray expression data was derived from six postmortem brains (one female, age: 24–57 years) provided by the Allen Human Brain Atlas (AHBA) [44]. The AHBA data was preprocessed and mapped to the Schaefer-400 atlas using the *abagen* toolbox [45], yielding a 400 (region) × 15,633 (gene) expression matrix.

Leveraging findings from a recently published genome-wide association study (GWAS) conducted by the ILAE Consortium [46], we extracted 43 risk genes linked to significant genome-wide loci in generalized epilepsy (Additional file 1: Table S2) [47]. We then analyzed the correlations between regional ALFF values and cortical expression levels of these genes derived from the AHBA [48]. Notably, this analysis was performed separately in GGE-GTCS patients and healthy controls to identify specific patterns associated with generalized epilepsy [48]. We identified 15 risk genes ($P_{spin} < 0.05$) that showed significant associations with ALFF values in GGE-GTCS but no significant correlations in the control group (Additional file 1: Table S3). Among the 43 risk genes, 15 disease-specific genes were used to calculate the gene expression gradient through principal component analysis (PCA). The principal axis (gene PC1) explained 48.78% of the total variance in gene expression, with *SCN9A* and *SCN1A* exhibiting high gene weights in PC1 (Additional file 1: Fig. S1).

Neurotransmitter receptor gradient

The principal axis of receptor density (receptor PC1) represents the primary variation of receptor density [14, 49]. Neurotransmitter receptor densities were constructed using open positron emission tomography (PET) tracer images from 1238 healthy participants (520 females) [50]. Receptor densities were acquired for 19 neurotransmitter receptors and transporters across nine neurotransmitter systems, namely serotonin (5-HT_{1A}, 5-HT_{1B}, 5-HT_{2A}, 5-HT_{4}, 5-HT_{6}, 5-HTT), dopamine (D_1, D_2, DAT), histamine (H_3), norepinephrine (NET), acetylcholine ($\alpha_4\beta_2$, M_1, VAChT), cannabinoid (CB_1), opioid (MOR), glutamate ($mGluR_5$, NMDA), and GABA ($GABA_A$) [50]. The volumetric PET images were registered to MNI space and parcellated into the Schaefer-400 atlas. Parcellated PET maps were standardized using z-scores normalization, yielding a 400 (region) × 19 (receptor/transporter) matrix. This matrix was applied to derive the receptor gradient through PCA, which captures 42.16% of the total variance in receptor density.

Excitatory/inhibitory ratio

The excitatory-inhibitory ratio for each region was calculated as the ratio between the average density of excitatory receptors and the average density of inhibitory receptors [14, 50]. Excitatory receptors include 5-HT_{2A},

5-HT_4, 5-HT_6, D_1, $\alpha_4\beta_2$, M_1, $mGluR_5$, and NMDA. Inhibitory receptors include 5-HT_{1A}, 5-HT_{1B}, CB_1, D_2, H_3, MOR, and $GABA_A$.

Laminar thickness gradient

The principal gradient of microstructural laminar thickness covariance (laminar PC1) represents the topographical variation in cytoarchitectural similarity across cortical laminae, and reflects changes in laminar differentiation and cytoarchitectural complexity [51, 52]. Laminar thickness was obtained from the BigBrain histological atlas of a post-mortem human brain (male, aged 65) [53]. The data was derived on "fsaverage" space using the BigBrainWarp toolbox [54], and parcellated into the Schaefer-400 atlas. The laminar similarity matrix was computed by pairwise partial correlation, controlling for mean laminar thickness across cortical regions [51, 52]. Finally, the principal axis of the laminar similarity was calculated by PCA, which explains 46.84% of the total variance in laminar thickness.

An element of the dependent variable was computed as the collective ALFF abnormality of structural neighbors of region *i*. The dependent variable characterized the extent to which the spatial patterning of ALFF abnormalities is constrained by SC (SC-constrained ALFF abnormalities). The predictor variables included four molecular profiles. We then estimated the relative importance of each molecular fingerprint in contributing to the overall fit of the linear regression model using dominance analysis in the R package *relaimpo* (v2.2–5) [55].

Network-based diffusion model and disease epicenter identification

To investigate whether abnormal transient neuronal activity spreads along the connectome via a diffusion process, we developed a network-based diffusion model [20] combining random walk and support vector regression (SVR). We first computed the diffusive probabilities of a seed region utilizing an *n*-step random walk algorithm [19] to depict the nodal diffusion characteristic at *n*th neighboring scales (see Additional file 1: Method S3 for details) [19, 20]. We then trained an SVR model at each neighboring scale to predict regional ALFF abnormalities using diffusive properties as input features. The model was trained by a tenfold cross-validation procedure with a linear kernel, and predictive performance was evaluated by calculating the Pearson correlation between empirical and predicted ALFF abnormalities at each scale.

To identify potential epicenters of ALFF abnormalities, we calculated the cosine similarity between the spatial patterns of ALFF abnormalities (*t*-values) and the diffusive properties of a seed region at each scale. The statistical significance was evaluated by applying a spin test [41, 42]. The regions were identified as putative disease epicenters if they showed significantly more spatial similarity than empirical similarity ($P_{spin} < 0.05$).

Associations with neuroimaging measures and clinical factors

We investigated the effects of various clinical factors on network-based spreading of brain activity abnormalities. Epilepsy is increasingly conceptualized as a dynamic pathological progression disease [56, 57]. We thus examined whether the relationships between brain activity abnormalities and structural connectome vary across different disease stages. To this end, we used a median split method [47] to categorize patients into two subgroups: short-duration patients (< 37 months, $n = 50$; 17 females; age = 24.50 ± 8.22 years) and long-duration patients (≥ 37 months, $n = 47$; 15 females; age = 25.30 ± 7.19 years). Disease duration-related ALFF abnormalities were identified by independently comparing ALFF differences in short- and long-duration patients with matched healthy controls. Subsequently, structural neighborhood analysis and epicenter models were re-computed for each disease stage and compared accordingly. Finally, we identified unique and shared epicenters across both disease stages.

Seizure frequency and antiepileptic medications may be implicated in the brain structure–function coupling of epilepsy [28, 58–60]. We investigated whether seizure frequency-related and medication-related brain activity abnormalities are constrained by connectome anatomy. We used a median split approach [47] to stratify patients into two subgroups based on seizure frequency: low-frequency patients (< 4 per year, $n = 43$; 11 females; age = 23.74 ± 7.15 years) and high-frequency patients (≥ 4 per year, $n = 44$; 15 females; age = 26.20 ± 8.01 years). Seizure frequency-related ALFF abnormalities were obtained by independently comparing ALFF differences in low- and high-frequency patients with matched healthy controls. Additionally, we divided patients into three subgroups based on the number of ASMs: no-medication group (ASMs = 0, $n = 28$; 11 females; age = 23.89 ± 6.03 years), monotherapy group (ASMs = 1, $n = 40$; 13 females; age = 25.40 ± 8.12 years) and polytherapy group (ASMs > 1, $n = 23$; 7 females; age = 24.78 ± 8.30 years). Medication-related ALFF abnormalities were identified by comparing each patient subgroup and matched healthy controls. Finally, we assessed the relationships between seizure frequency-related and medication-related brain activity abnormalities and their directly structurally connected neighbor.

Patient-tailored activity abnormality modeling

We examined whether network-based models could be generalized to individual patients with GGE-GTCS and

how individual clinical variables influenced them. First, we used normative modeling [61] to obtain patient-specific ALFF deviation *W*-score maps. Specifically, we used multivariate linear models with age and sex as covariates to generate a normative model of ALFF values from healthy participants. Each patient's empirical ALFF values were compared against model estimates to generate region-wise *W*-score maps. Then, we calculated patient-specific correlations between individual *W*-scores and the average scores of their structurally connected neighbors. We assessed the relationships between these subject-level correlations and clinical features, including disease duration, seizure onset age, seizure frequency, and the number of ASMs. Finally, we identified each patient's disease epicenters as those regions where diffusive properties exhibited a significant cosine similarity with the patient's ALFF deviation *W*-score maps. Subject-level network modeling could identify fluctuations that may be linked to pathologically relevant variables, which is crucial for advancing the clinical translation of our approach [28, 62].

Sensitivity and replication analyses

We performed additional analyses to verify the robustness of the main results. First, to measure the effect of structural connectome threshold selection on predicting neighborhood ALFF abnormalities, we repeated the analyses using three thresholds (i.e., SC values higher than 0.3, 0.4, and 0.5). Second, we considered the associations between regional ALFF abnormality and the average abnormality observed in non-connected structural neighborhood regions to investigate the spatial proximity effect. Third, we repeated the analysis after regressing Euclidean distance to ensure that distance alone did not affect connected neighborhood ALFF abnormalities. Finally, we repeated the main analyses using the Schaefer-100 and Schaefer-800 atlases [36].

We further replicated the main analyses using the split-half analysis [63, 64]. We divided patients into two subgroups: GGE-GTCS1 ($n=49$; 16 females; age = 25.06 ± 7.71 years) and GGE-GTCS2 ($n=48$; 16 females; age = 24.71 ± 7.79 years), and demographically matched health controls (HC1: $n=71$; 31 females; age = 25.51 ± 6.27 years; HC2: $n=70$; 31 females; age = 25.43 ± 6.46 years) (all $P>0.05$). We performed case–control ALFF difference (*t*-value) maps on the subgroups (i.e., GGE-GTCS1 vs. HC1, and GGE-GTCS2 vs. HC2), while controlling for age, sex, and mFD. We then computed spatial correlation for the *t*-maps between subgroups and the main result. Furthermore, we performed structural neighborhood analysis and disease epicenter identification for each subgroup analogously to the whole-group analysis.

Results

System-specific abnormalities of brain activity

We constructed whole-cortex difference (*t*-value) maps of ALFF between patients with GGE-GTCS and matched controls using a general linear model (Fig. 1A). We identified 18 cortical regions with significant ALFF differences, of which 17 showed stronger activity (increased) in GGE-GTCS (positive *t*-values) (Fig. 1B). These hyperactive regions were located primarily in the temporal, cingulate, prefrontal, and parietal cortices, whereas spontaneous activity was weaker (negative *t*-values) in the left inferior parietal area (all $P_{FDR}<0.05$; Additional file 1: Table S4).

We assessed the relationships between ALFF values of significantly abnormal regions and clinical variables (Additional file 1: Table S5). We found that the right paracentral lobule and right middle cingulate cortex ($P_{FDR}<0.05$) exhibited negative correlations with the duration of illness. The left anterior cingulate cortex, right inferior parietal lobule, right precuneus, and right middle cingulate cortex ($P_{FDR}<0.05$) negatively correlated with seizure onset age. Moreover, the right inferior parietal lobule ($P_{FDR}<0.05$) also negatively correlated with the number of ASMs. In contrast, no significant correlations ($P_{FDR}>0.05$) were found with the seizure frequency. These findings suggest that brain activity in GGE-GTCS may be progressively inhibited with increasing disease duration and more ASMs.

We further investigated whether these ALFF abnormalities were pronounced in specific brain systems. Among intrinsic functional networks [39] (Fig. 1C), the group difference in ALFF was stronger within the somatomotor network (*z*-score = 2.06, $P_{FDR}=0.024$) and weaker within the default mode network (*z*-score = -2.15, $P_{FDR}=0.016$). Among laminar differentiation classes [40] (Fig. 1D), differences were greater in the idiotypic class (*z*-score = 2.32, $P_{FDR}=0.016$) and lower in the heteromodal laminar class (*z*-score = -2.246, $P_{FDR}=0.008$) compared to the null distributions. Consistent results were found at the other two parcellation resolutions (Additional file 1: Fig. S2 and S3). Collectively, neuronal activity abnormalities in patients with GGE-GTCS were most pronounced in the primary sensorimotor cortices and relatively weaker in high-order association cortices.

Structural connectome constrains abnormalities of brain activity

We tested whether the distribution of ALFF abnormalities was conditioned by structural connectome. We evaluated the relationships between regional ALFF abnormality (*t*-value) and the average abnormality of structurally connected neighbors (Fig. 2A),

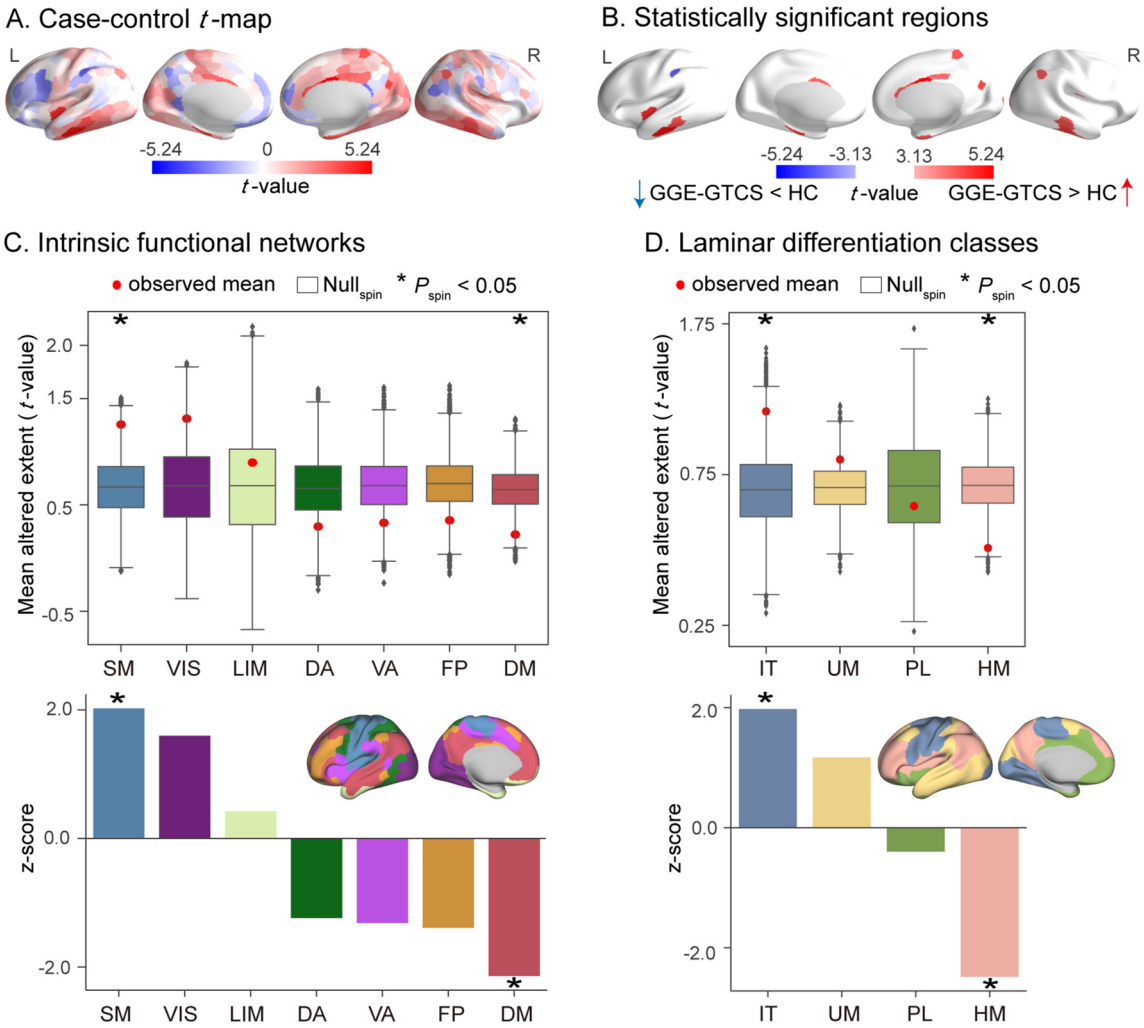

Fig. 1 The spatial patterning of ALFF abnormalities in GGE-GTCS. **A** Case–control comparison of regional ALFF (*t*-value, unthresholded). **B** Eighteen cortical areas showed statistically significant differences in ALFF ($P_{FDR} < 0.05$). **C** and **D** Each system's mean ALFF alteration scores were calculated for Yeo intrinsic functional networks [39] and Mesulam laminar differentiation classes [40]. The observed mean difference scores (red circles) were compared to the null distribution of mean difference magnitudes generated through spin tests [41, 42] (boxplots; 10,000 repetitions; $P_{spin} < 0.05$, two-tailed; FDR-corrected). The mean *t*-values of each system were converted to *z*-scores relative to the null distribution. A positive *z*-score represents a greater difference than expected, and vice versa. List of intrinsic functional networks: DA, dorsal attention; DM, default mode; FP, frontoparietal; LIM, limbic; SM, somatomotor; VIS, visual; VA, ventral attention. List of laminar differentiation classes: HM, heteromodal; IT, idiotypic; PL, paralimbic; UM, unimodal

which revealed a significant positive spatial correlation ($r = 0.55$, $P_{spin/rewired} < 0.001$; Fig. 2B), suggesting that spatial patterning of ALFF abnormalities in patients with GGE-GTCS reflects the underlying structural connectome architecture. Furthermore, the direct structural connectome within heteromodal cortices, particularly within and between the limbic and default mode networks, conferred significant constraints on these ALFF abnormalities among patients, indicating that SC constrains aberrant neuronal activity at the systems levels (Fig. 2C).

We repeated the analyses with three different connection thresholds (Additional file 1: Fig. S4), confirming that correlations were not biased by the choice of a particular connection threshold. In addition, the correlations between structurally connected neighbors were significantly higher than those for structurally disconnected neighbors. Furthermore, we regressed the mean Euclidean distance between a given region and its connected neighbors, showing that observed correlations were not affected by the effect of spatial proximity (Additional file 1: Table S6). These findings were consistent

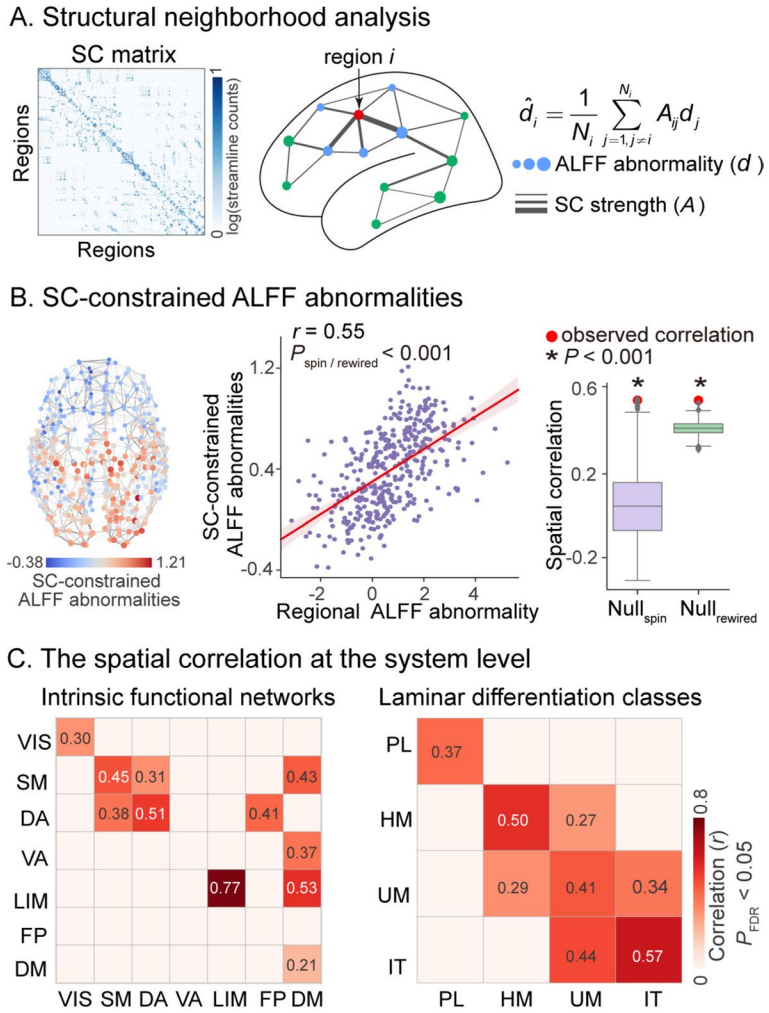

Fig. 2 Normative structural connectome (SC) constrains ALFF abnormalities in GGE-GTCS. **A** Schematic diagram of structural neighborhood analysis [13]. The collective ALFF abnormality of structural neighbors for a given region (red) was modeled as the average abnormality of its directly structurally connected neighbors (blue). **B** SC-constrained ALFF abnormalities. Brain rendering shows the associations between ALFF abnormalities and SC. The edge thickness on the brain plot indicates the SC strength, and the node size and color represent the degree of SC constraint on ALFF abnormalities (i.e., the larger and redder, the greater the constraint degree). The scatterplot reveals a significant correlation between regional ALFF abnormality and that of structurally connected neighbors. The boxplots show the observed correlation against surrogate correlations generated from spin tests [41, 42] ("$\text{Null}_{\text{spin}}$," 10,000 repetitions) and rewired tests [65, 66] ("$\text{Null}_{\text{rewired}}$," 1000 repetitions). Asterisks denote statistical significance (*$P < 0.001$, one-tailed). **C** The spatial correlation at the system levels. The statistically significant correlations are depicted in red ($P_{\text{spin}} < 0.05$, one-tailed, FDR-corrected). List of intrinsic functional networks: DA, dorsal attention; DM, default mode; FP, frontoparietal; LIM, limbic; SM, somatomotor; VIS, visual; VA, ventral attention. List of laminar differentiation classes: HM, heteromodal; IT, idiotypic; PL, paralimbic; UM, unimodal

across all three parcellation resolutions (Additional file 1: Fig. S5), proving that structural connectome architecture shapes the spatial distribution of ALFF abnormalities in GGE-GTCS.

We investigated whether brain activity abnormalities related to clinical factors are constrained by the structural connectome. We found that ALFF abnormalities associated with disease duration were significantly correlated with structurally connected neighbors in short-duration ($r = 0.57$, $P_{\text{spin/rewired}} < 0.001$) and long-duration ($r = 0.48$, $P_{\text{spin/rewired}} < 0.001$) groups (Additional file 1: Fig. S6), suggesting that ALFF alterations may be strongly constrained by connectome architecture in early illness stages. Similarly, the collective abnormalities of structurally connected neighbors were correlated with seizure frequency-related ALFF abnormalities in patients with low-frequency ($r = 0.37$, $P_{\text{spin/rewired}} < 0.001$) and high-frequency ($r = 0.53$, $P_{\text{spin/rewired}} < 0.001$) groups (Additional file 1: Fig. S7). Additionally, medication-related ALFF abnormalities were correlated with their structurally

connected neighbors in patients receiving no medication ($r=0.42$, $P_{spin/rewired}<0.001$), monotherapy ($r=0.49$, $P_{spin/rewired}<0.001$), and polytherapy ($r=0.51$, $P_{spin/rewired}<0.001$) (Additional file 1: Fig. S8). These findings suggest that higher epilepsy severity may be linked to more profound manifestations of network spreading of abnormal brain activity. Consequently, the structural connectome represents a fundamental constraint on illness-related ALFF abnormalities in GGE-GTCS.

Molecular fingerprints associated with SC-constrained activity abnormalities

We next investigated whether molecular fingerprints modulate the constraints imposed by the SC on ALFF abnormalities. A multilinear regression model (Fig. 3A) was constructed to determine the relationships between SC-constrained ALFF abnormality patterns and molecular fingerprints, including disease-related gene expression gradient, neurotransmitter receptor gradient, excitatory/inhibitory ratio, and laminar thickness gradient (Fig. 3B). The dependent variable was SC-constrained ALFF abnormalities, which represents the degree to which SC constrains the spatial patterning of ALFF abnormalities.

The regression model explained 27.16% of the variance in the constraints of ALFF abnormalities by the SC ($F_{(4,395)}=36.81$, $P_{spin}<0.001$). We found a significant positive correlation between observed and fitted SC-constrained ALFF abnormalities ($r=0.52$, $P_{spin}<0.01$) (Fig. 3C). Dominance analysis revealed that laminar thickness gradient ($P_{spin}=0.029$, FDR-correction) and neurotransmitter receptor gradient ($P_{spin}=0.038$, FDR-correction) are the important predictors in the model, with laminar thickness profile (56.75%) showing the most considerable dominance (Fig. 3D; Additional file 1: Table S7). These findings suggest that molecular fingerprints contribute to the constraints of ALFF abnormalities by the structural connectome.

Network-based spreading and disease epicenters

The strong associations between ALFF abnormalities and structural network suggest that pathological activity propagates along the connectome. However, structural neighborhood analysis provides limited insights into the spreading processes and fails to identify disease epicenters. Thus, we next applied a network-based diffusion model [20] to explore whether these disease-associated ALFF abnormalities propagate along the connectome via a diffusion process and whether specific brain regions function as epicenters of this spread.

The diffusion processes across multiscale structural network edges were applied to predict the abnormal activity patterns. First, we generated the nodal diffusion

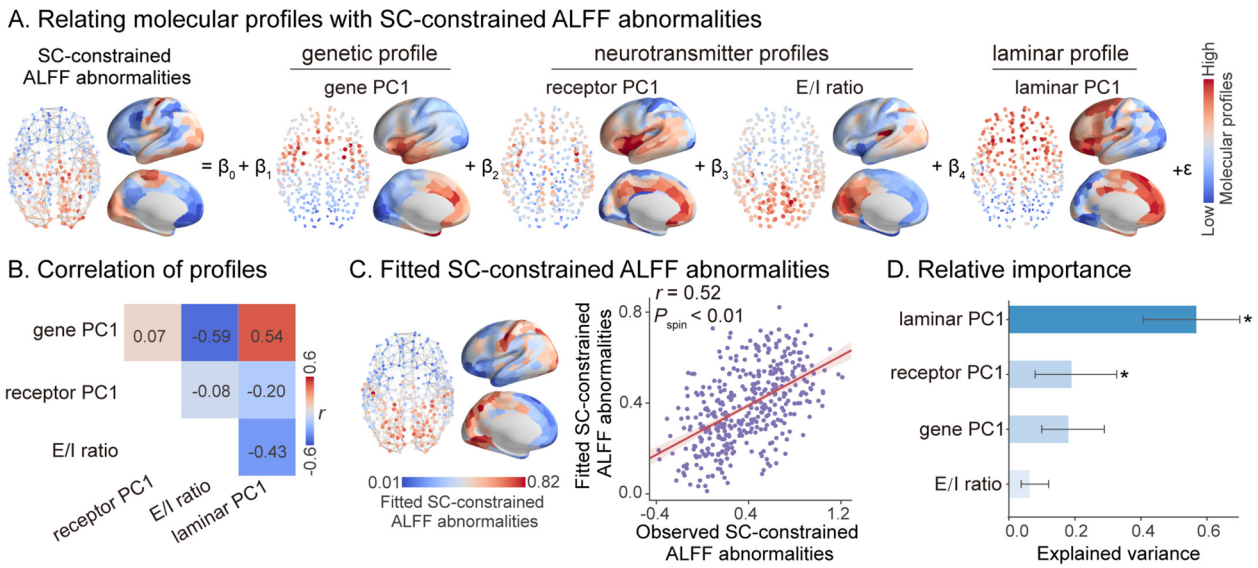

Fig. 3 Molecular profiles contributing to structural connectome (SC)-constrained ALFF abnormalities in GGE-GTCS. **A** A multiple linear regression model was constructed to determine the relationships between regional heterogeneous constraints and molecular profiles. **B** Heatmap shows Pearson's correlation coefficients between pairs of molecular profiles. **C** The scatter plot displays the relationship between observed and fitted SC-constrained ALFF abnormalities. **D** Dominance analysis was used to evaluate the relative importance of molecular profiles to the fit of the model. Error bars represent 95% bootstrap confidence intervals (10,000 repetitions). Asterisks denote the statistical significance regression coefficient (*$P_{spin}<0.05$, FDR-correction). Gene PC1, first component of 15 disease-related gene expression; Receptor PC1, first component of 19 neurotransmitter receptor densities; E/I ratio, excitatory/inhibitory receptor density ratio; Laminar PC1, first component of laminar thickness covariance

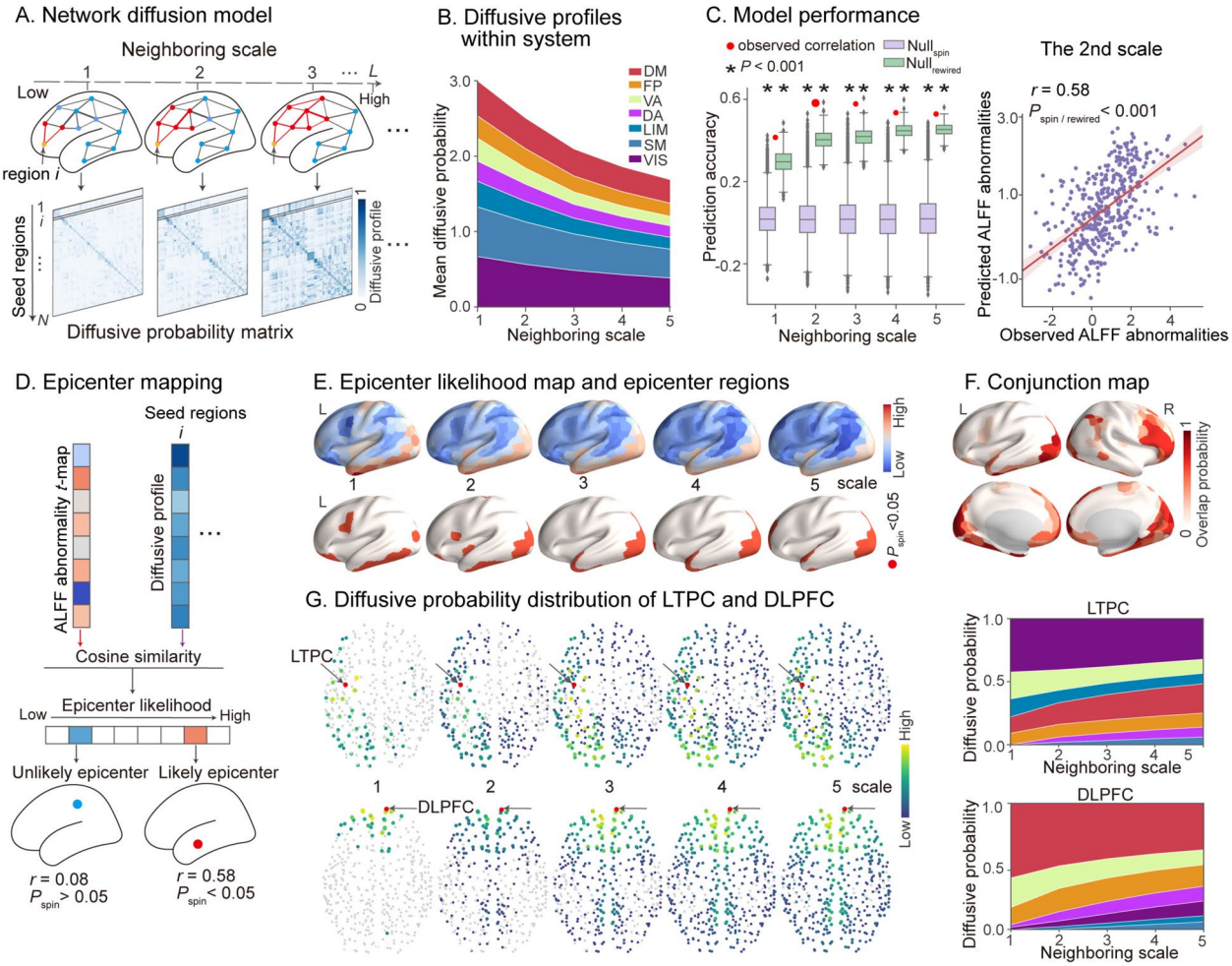

Fig. 4 Network-based spreading of ALFF abnormalities and epicenter identification in GGE-GTCS. **A** Schematic illustration of the network-based diffusion model [20]. The red nodes and edges represent the *n*th neighboring scale of a given region (orange). **B** The mean diffusive probability curves within the same system in Yeo intrinsic functional networks. **C** Model predictive performance. The empirical correlations (red circles) were compared to surrogate correlations generated from spin tests ("$Null_{spin}$," 10,000 repetitions) and rewired tests ("$Null_{rewired}$," 1000 repetitions). Asterisks denote statistical significance (*$P < 0.001$, one-tailed). The scatter plot displays the best predictive performance at the second neighboring scale. **D** Schematic of the disease epicenter mapping approach [20]. **E** The epicenter likelihood maps (*top* panels) and epicenter regions (*bottom* panels; $P_{spin} < 0.05$, one-tailed) at five neighboring scales. **F** The conjunction map of disease epicenters illustrates the probability of each region being recognized as an epicenter across five scales. **G** Diffusive probability distribution of two robust epicenters depicted in the limbic-temporal cortex (LTPC, *top* panels) and dorsolateral prefrontal cortex (DLPFC, *bottom* panels) at each scale. The *right* panels display the diffusive probability of two epicenters within and between networks. DA, dorsal attention; DM, default mode; FP, frontoparietal; LIM, limbic; SM, somatomotor; VIS, visual; VA, ventral attention

characteristic at *n*th neighboring scales using a random walk algorithm (Fig. 4A) [19, 20]. Second, we computed the mean diffusive probabilities within the same Yeo intrinsic functional network (Fig. 4B), which revealed that diffusion probability decreased with neighboring scales, suggesting greater system segregation at smaller scales during the diffusion process. Third, we performed SVR prediction of ALFF abnormalities using diffusion features, and found that predicted disease patterns were significantly related to ALFF abnormalities in GGE-GTCS across five neighboring scales ($r_{1-5\ scale}$ ranged from 0.42 to 0.58, all $P_{spin/rewired} < 0.001$). Specially, the second neighboring scale showed the highest predictive performance ($r = 0.58$, $P_{spin/rewired} < 0.001$; Fig. 4C). The highest positive contributive features were in the somatomotor and limbic networks, and the highest negative contributive features were in the dorsal attention and default mode networks (Additional file 1: Fig. S9). These findings remained consistent across all three resolutions (Additional file 1: Fig. S10). Therefore, the multiscale

diffusion profiles of structural networks largely shape the spatial patterning of ALFF abnormalities in GGE-GTCS.

We constructed epicenter likelihood maps by calculating the cosine similarity between regional ALFF abnormalities and the diffusive properties for each seed region at *n*th neighboring scales (Fig. 4D). These epicenter likelihood maps exhibited similarity across five neighboring scales, with regions of high similarity corresponding to the fusiform gyrus, occipital gyrus, inferior temporal gyrus, and prefrontal cortices (Fig. 4E). Furthermore, regions with significantly higher spatial similarities were identified as potential epicenters. The conjunction map of epicenters across five scales revealed that the most stable epicenters were predominantly in the limbic-temporal cortex (LTPC), dorsolateral prefrontal cortex (DLPFC), and occipital cortex (Fig. 4F; Additional file 1: Fig. S11), suggesting that these regions are dominant drivers of pathological spread in GGE-GTCS. Similar results were obtained using other parcellation resolutions (Additional file 1: Fig. S12).

To illustrate the pathological spread processes from epicenters at each neighboring scale, we constructed the diffusive distribution of the two most robust epicenters in the LTPC (Fig. 4G, *top* panels) and DLPFC (Fig. 4G, *bottom* panels). With the expansion of the neighborhood scale, LTPC pathology spread mainly to visual (VIS), default mode (DM), and ventral attention (VA) systems, and DLPFC pathology spread primarily to DM, VA, and frontoparietal (FP) systems. These results indicate system separation at small neighboring scales and system integration at large neighboring scales during the spread of pathology in GGE-GTCS.

We further identified the epicenters of abnormal brain activity at different stages of disease duration. Based on previous evidence of network-based disease progression [15, 16, 62, 67], we hypothesized that these epicenters would exhibit spatial propagation from some regions to broader network areas with disease progression. The convergent epicenters across two disease stages were primarily localized in the occipital, limbic-temporal, and lateral prefrontal cortices (Additional file 1: Fig. S13). Notably, we observed a progressive spatial shift in epicenter localization with increasing disease duration, characterized by a transition from orbitofrontal and prefrontal cortices in early stages to temporal and parietal cortices in later stages, reflecting the network-based spreading of abnormal brain activity across different stages of GGE-GTCS.

Patient-tailored activity abnormality modeling

Next, we assessed the generalizability of network-based models for individual patients with GGE-GTCS. Although the subject-level data showed lower sensitivity due to increased heterogeneity in ALFF patterns among patients, we found that patient-specific correlations between individual ALFF deviations and their directly structurally connected neighbors closely mirrored the group-level findings (Additional file 1: Fig. S14A). Notably, these correlations were significant for almost all patients with GGE-GTCS (r ranged from 0.27 to 0.74; $P_{spin} < 0.05$ in all individuals, and $P_{rewired} < 0.05$ in 84.54% of individuals). Similarly, disease epicenters were consistent across individual patients, with the prefrontal and occipital cortices being the most common locations in GGE-GTCS (Additional file 1: Fig. S14B). Individual level of SC-constrained ALFF vulnerability indicated by patient-specific higher positive correlation coefficients was consistently associated with seizure frequency ($r = 0.22$, $P = 0.038$). No significant association was observed with either disease duration, seizure onset age, or the number of ASMs (Additional file 1: Fig. S15).

Reproducibility analysis

We further carried out split-half analyses to test the reproducibility of our main results. The results of subgroup analysis were highly consistent with those obtained using whole-group analysis (Additional file 1: Fig. S16). We observed that the spatial *t*-maps were similar between GGE-GTCS1 vs. HC1 and the main result ($r = 0.89$, $P_{spin} < 0.001$), as well as between GGE-GTCS2 vs. HC2 and the main result ($r = 0.88$, $P_{spin} < 0.001$). Regional ALFF abnormality (*t*-value) significantly correlated with the collective abnormality of structurally connected neighbor for each subgroup (GGE-GTCS1: $r = 0.58$; GGE-GTCS2: $r = 0.43$; all $P_{spin/rewired} < 0.001$). Moreover, disease epicenters were mainly located in the limbic-temporal, prefrontal, and occipital cortices. Collectively, these results suggest a high reproducibility of our findings.

Discussion

We demonstrated that structural connectome architecture provides a conduit for the spread of transient neuronal activity in GGE-GTCS and that local molecular attributes influence this process. Furthermore, network-based diffusion modeling effectively simulated the pathological spread of abnormal transient activity, identifying the limbic-temporal, prefrontal, and occipital cortices as putative epicenters. These results were repeatable across different clinical variables and individual patients.

Brain activity abnormalities in patients with GGE-GTCS were most pronounced in the sensorimotor network and relatively less prominent in the default mode network (DMN). Convergent evidence from simultaneous EEG-fMRI studies has reported abnormal neuronal activity in both the sensorimotor network and the DMN of epileptic patients [68–70]. The sensorimotor network

demonstrated functional activity hypersynchrony, which has been characterized as a state-independent endophenotype of GGE [69]. The synchronization of unbalanced activity within the sensorimotor network may propagate across large-scale brain circuits, ultimately leading to generalized seizures [69]. Moreover, previous studies have shown abnormal motor task-induced activation in GGE, providing evidence that the susceptibility of the motor system plays a pivotal role in the instability of the epileptic brain state [71, 72]. Alternatively, DMN dysfunction has been widely implicated in consciousness and cognitive impairments pathophysiology. Consistent with prior findings [68, 70], the weaker neuronal activity observed in the DMN of the patients may indicate a temporary suspension of the default state of brain function. This specific pattern of aberrant activity may explain the transient loss or disturbance of awareness during generalized epileptic seizures concomitant with sensorimotor symptoms [73]. Collectively, these findings highlight the critical role of specific brain networks in shaping the spatial patterning of neuronal activity abnormalities in GGE-GTCS.

The topology of the structural connectome constrains the spatial patterning of ALFF abnormalities in GGE-GTCS. Previous studies have similarly shown that brain morphometric abnormalities in neurological and psychiatric disorders were conditioned by the underlying network architecture [13–15, 62, 74]. Our results suggest that the collective abnormalities of structurally connected neighborhoods can predict cross-sectional ALFF differences. These results were confirmed by multiple recent studies [28, 75, 76]. Structural organization influenced the pathological spread of large-scale brain activity waves in epilepsy [28]. Structural disconnections within and between hemispheres may contribute to pathogenic activity synchronization [75]. Moreover, the atypical organization of functional activity was partially driven by white matter microstructure alterations [76]. Beyond cross-sectional differences, our results further showed that brain activity abnormalities related to disease duration, seizure frequency, and medication exposure are also constrained by connectome architecture, suggesting that network organization may guide brain activity dysfunction at different clinical factors of GGE-GTCS. Therefore, understanding disease onset and progression requires elucidation of how the structural connectome influences the pathology propagation. In the case of GGE-GTCS, this requires greater knowledge of how ALFF abnormalities propagate along specific vulnerable axonal tracts.

We also found that multiple molecular features regulate the constraints imposed by the structural connectome on ALFF abnormalities. White matter tracts transmit neural activity (action potentials) and molecules essential for growth, plasticity, and repair, including neurotransmitter receptors, kinases, transporters, and neurotrophic/growth factors [77]. Numerous studies have indicated that pathological synaptic development, plasticity, and signaling in GGE-GTCS may be due to genetic mutations [78], neurotransmission system alterations [79], and cortical microstructural changes [80]. The heterogeneity of molecular profiles across the brain may predispose specific regions to epilepsy, ultimately leading to disease onset and progression [14]. The disease-specific gene expression gradient represents a hierarchy of transcriptomic specialization and reflects the possible pathophysiology of generalized epilepsy [43, 81]. Bridging macroscale neuroimaging phenotypic variations with microscale gene expression profiles may reveal the relationships between specific transcriptomic signatures and GGE-GTCS pathology [64]. Furthermore, neurotransmitter receptor gradients indicate that individual brain regions process endogenous signals differently, which may confer greater or less susceptibility to epilepsy [14]. Aberrant changes in receptor profiles may play a critical role in the pathogenesis of epilepsy, particularly those shifting the excitatory and inhibitory balance [78, 79]. Additionally, topographic variations in cortical microstructure gradient reflect large-scale laminar organization [51, 52], potentially providing insights into how laminar differentiation disruptions contribute to abnormal neural activity and seizure propagation [80]. Therefore, elucidating the relationships between molecular fingerprints and connectome-constrained ALFF abnormalities may help advance our understanding of GGE-GTCS pathogenesis.

We applied a network-based diffusion model to simulate the spreading of abnormal transient activity in GGE-GTCS. Pathological perturbations often propagate from focal lesions through axonal pathways, ultimately impacting the functioning of more extensive networks [9]. Numerous network-based diffusion models have been used successfully to describe the progressive spread of pathological events along the brain connectome [18, 19]. For instance, these diffusive models have revealed that the progression of brain atrophy follows the connectome. In line with these findings [18–20], our network diffusion model, combining random walks and machine learning, successfully simulated the spatial patterns of ALFF abnormalities in GGE-GTCS, suggesting that the propagation of other pathogenic processes may be simulated using the knowledge of network topology. Importantly, we found that anatomically connected neighbors determined the pattern of regional activity vulnerability, which could be explained by polysynaptic communication between distant anatomically connected neurons [19]. Therefore, the structural connectome's multiscale

diffusion profiles constrain the ALFF abnormalities spread in GGE-GTCS.

We further identified potential epicenters of ALFF abnormalities in GGE-GTCS using this diffusion model, thereby providing additional support for the notion that the structural connectome guides the spread of pathology [8]. The most common epicenter locations were limbic-temporal, dorsolateral prefrontal, and occipital cortices. Illness duration-related epicenters were apparent in orbitofrontal and prefrontal cortices early in the illness and shifted to temporal and parietal cortices with illness progression. The occipital, limbic-temporal, and lateral prefrontal cortices consistently emerged as potential epicenters across disease stages. These regions are frequently implicated in GGE-GTCS due to abnormalities in cortical morphometry [64], white matter fiber bundle organization [82], intrinsic brain activity [4–6], and functional connectivity [32]. The limbic-temporal cortex is responsible for critical processes such as auditory processing, memory, and emotion and is among the most epilepsy-prone regions of the human brain [83]. Similarly, a meta-analysis identified the dorsolateral prefrontal cortex as a common epicenter in GGE based on morphological abnormalities [8]. Furthermore, the involvement of the occipital cortex as an epicenter may explain the deficits in higher social perception based on dynamic social cues in GGE, as the so-called third visual pathway mediates these functions [84]. Together, our findings suggest that limbic-temporal, dorsolateral prefrontal, and occipital cortices drive the onset and spread of GGE-GTCS-associated pathology.

This study has several methodological limitations. First, the case–control design precludes causal inferences on the associations of connectome structure with patterns of abnormal neuronal activity in GGE-GTCS. Specifically, it is still uncertain whether abnormal spontaneous neural activity drives structural disconnection or if white matter lesions alter regional spontaneous activity in patients with GGE-GTCS [82]. Second, our analyses did not include subcortical areas contributing to generalized epilepsy [85]. Third, since local abnormal intrinsic activity may alter the connectivity with other regions, we constructed the connectome from the DWI data of a healthy population. However, widespread changes in the structural networks of GGE-GTCS patients may reroute the spread of pathology [86]. Future studies are needed to examine how the individual patient's structural connectome impacts the pathology's spread. Fourth, molecular fingerprints were also derived from publicly available datasets in healthy populations. Still, they may not fully capture individual variability [14], which is critical for understanding the pathophysiology of GGE-GTCS. Future studies should investigate how disease-associated molecular fingerprints influence the spread of pathology in GGE-GTCS. Finally, future works should incorporate neuropsychological testing to assess cognitive and behavioral deficits and explore the relationships between structure–function network spreading and cognitive performance [27–29].

Conclusions

In summary, we demonstrated that large-scale structural connectome architecture constrains the spread of abnormal brain activity in GGE-GTCS and that local molecular attributes can modulate these constraints. The limbic-temporal, dorsolateral prefrontal, and occipital cortices may be common epicenters of pathological spread. Collectively, these findings enhance our understanding of the network-level mechanisms controlling the spread of pathological brain activity in GGE-GTCS.

Abbreviations

AHBA	Allen Human Brain Atlas
ALFF	Amplitude of low-frequency fluctuations
ASMs	Antiseizure medications
DWI	Diffusion-weighted imaging
DMN	Default mode network
EEG	Electroencephalogram
FD	Frame-wise displacement
FDR	False discovery rate
fMRI	Functional magnetic resonance imaging
GGE-GTCS	Genetic generalized epilepsy with tonic–clonic seizure
HCs	Healthy controls
PCA	Principal component analysis
PET	Positron emission tomography
SC	Structural connectome
SVR	Support vector regression

Supplementary Information

The online version contains supplementary material available at https://doi.org/10.1186/s12916-025-04099-7.

Additional file 1. Supplementary Methods. Method S1. Null models. Method S2. Structural neighborhood analysis; Method S3. Network-based diffusion model. Figures S1-S16. Tables S1-S7. Fig. S1. Principal component loadings of disease-specific gene expression. Fig. S2. The spatial patterning of ALFF abnormalities in GGE-GTCS at Schaefer-100 atlas. Fig. S3. The spatial patterning of ALFF abnormalities in GGE-GTCS at Schaefer-800 atlas. Fig. S4. Replicable SC-constrained ALFF abnormalities under different connection thresholds. Fig. S5. Replicable structural SC-constrained ALFF abnormalities. Fig. S6. SC constrains duration-related ALFF abnormalities in GGE-GTCS. Fig. S7. SC constrains seizure frequency-related ALFF abnormalities in GGE-GTCS. Fig. S8. SC constrains medication-related ALFF abnormalities in GGE-GTCS. Fig. S9. Feature weights for the SVR model. Fig. S10. Network diffusion model at Schaefer-100 and Schaefer-800 parcellation atlases. Fig. S11. Disease epicenters at Schaefer-400 parcellation atlas. Fig. S12. Disease epicenters at Schaefer-100 and Schaefer-800 parcellation atlases. Fig. S13. Duration-related epicenters in GGE-GTCS. Fig. S14. Patient-tailored ALFF abnormality modeling. Fig. S15. Associations between subject-level network modeling and individual clinical features. Fig. S16. Validation results using split-half analyses. Table S1. Demographic and clinical characteristics. Table S2. List of disease-specific risk genes in generalized epilepsy. Table S3. The correlations between the expression levels of risk genes and regional ALFF values. Table S4. Regions showing abnormal ALFF in patients with GGE-GTCS. Table S5. Associations between clinical variables and regional ALFF values in patients with

GGE-GTCS. Table S6. Results of node-neighbor relationship for connected versus not-connected neighbors. Table S7. Results of the relationships between molecular fingerprints and SC-constrained ALFF abnormalities in GGE-GTCS.

Acknowledgements
We thank International Science Editing (http://www.internationalscienceediting.com) for editing this manuscript.

Authors' contributions
W.L. and H.C. supervised the study. J.X. and W.L. designed the methodology and implemented the visualization. Z.Z. organized the MRI data. Y.M. and S.Y. processed the MRI data. J.L. and J.N. contributed and implemented the investigation. J.X., W.L., and S.Y. wrote and edited the manuscript. All authors read and approved the final manuscript.

Authors' Twitter handles
Twitter handles: @WeiLiao81 (Wei Liao), @jiexia32713535 (Jie Xia).

Funding
This study was supported by the National Key R&D Program of China (2022YFC2009906 (W.L.) and 2022YFC2009900 (W.L.)), the National Natural Science Foundation of China (62036003 (H.C.), 82121003 (H.C.), 62333003(H.C.), 62473082 (J.L.), 82202250 (J.L.), and 82302293 (S.Y.)), the Fundamental Research Funds for the Central Universities (ZYGX2022YGRH008 (W.L.)), the Medical-Engineering Cooperation Funds from the University of Electronic Science and Technology of China (ZYGX2021YGLH201 (H.C.)), and the Science and Technology foundation of Sichuan Province (2024NSFSC1782 (S.Y.)).

Data availability
The HCP dataset [34] is available at https://db.humanconnectome.org/. The microarray gene expression data [43] is publicly available at https://human.brain-map.org/. The receptor density atlas [50] is available at https://github.com/netneurolab/hansen_receptors. And the BigBrain data [53] is available at https://bigbrainwarp.readthedocs.io. The code of the network-based model [20] is available at https://github.com/Xinyuan-Liang/SC-shapes-the-maturation-of-cortical-morphology. Genetic data were preprocessed with the abagen toolbox (https://github.com/netneurolab/abagen) [45]. The spin test [41, 42] was conducted using an open package (https://github.com/frantisekvasa/rotate_parcellation). The rewired network [65, 66] null models were generated using an open package (https://www.brainnetworkslab.com/coderesources). The brain surfaces were visualized using netneurotools (https://github.com/netneurolab/netneurotools) [87].

Declarations

Ethics approval and consent to participate
The study has been approved by the medical ethics committee of Jinling Hospital, School of Medicine, Nanjing University, China (approval number: 2014GJJ-056). Written informed consent was obtained from all participants in accordance with the Declaration of Helsinki.

Consent for publication
Not applicable.

Competing interests
The authors declare no competing interests.

Author details
[1]The Clinical Hospital of Chengdu Brain Science Institute, School of Life Science and Technology, University of Electronic Science and Technology of China, Chengdu 611731, People's Republic of China. [2]MOE Key Lab for Neuroinformation, High-Field Magnetic Resonance Brain Imaging Key Laboratory of Sichuan Province, University of Electronic Science and Technology of China, Chengdu 611731, People's Republic of China. [3]School of Cybersecurity, Chengdu University of Information Technology, Chengdu 610225, People's Republic of China. [4]Department of Medical Imaging, Jinling Hospital, Nanjing University School of Medicine, Nanjing 210002, People's Republic of China.

Received: 27 November 2024 Accepted: 24 April 2025
Published online: 02 May 2025

References

1. Fisher RS, Cross JH, French JA, Higurashi N, Hirsch E, Jansen FE, Lagae L, Moshé SL, Peltola J, Roulet PE. Operational classification of seizure types by the International League Against Epilepsy: Position Paper of the ILAE Commission for Classification and Terminology. Epilepsia. 2017;58(4):522–30.
2. Devinsky O, Elder C, Sivathamboo S, Scheffer IE, Koepp MJ. Idiopathic generalized epilepsy: misunderstandings, challenges, and opportunities. Neurology. 2024;102(3): e208076.
3. Zang Y-F, He Y, Zhu C-Z, Cao Q-J, Sui M-Q, Liang M, Tian L-X, Jiang T-Z, Wang Y-F. Altered baseline brain activity in children with ADHD revealed by resting-state functional MRI. Brain Dev. 2007;29(2):83–91.
4. Liao W, Wang J, Xu T, Zhang Z, Ji G-J, Xu Q, Wang Z, Yang F, Zuo X-N, Qiu A. Altered relationship between thickness and intrinsic activity amplitude in generalized tonic–clonic seizures. Sci Bull. 2016;61:1865–75.
5. Wang Z, Zhang Z, Liao W, Xu Q, Zhang J, Lu W, Jiao Q, Chen G, Feng J, Lu G. Frequency-dependent amplitude alterations of resting-state spontaneous fluctuations in idiopathic generalized epilepsy. Epilepsy Res. 2014;108(5):853–60.
6. McGill ML, Devinsky O, Wang X, Quinn BT, Pardoe H, Carlson C, Butler T, Kuzniecky R, Thesen T. Functional neuroimaging abnormalities in idiopathic generalized epilepsy. NeuroImage Clin. 2014;6:455–62.
7. Engel J, Thompson PM, Stern JM, Staba RJ, Bragin A, Mody I. Connectomics and epilepsy. Curr Opin Neurol. 2013;26(2):186–94.
8. Lariviere S, Rodríguez-Cruces R, Royer J, Caligiuri ME, Gambardella A, Concha L, Keller SS, Cendes F, Yasuda C, Bonilha L. Network-based atrophy modeling in the common epilepsies: A worldwide ENIGMA study. Sci Adv. 2020;6(47):eabc6457.
9. Fornito A, Zalesky A, Breakspear M. The connectomics of brain disorders. Nat Rev Neurosci. 2015;16(3):159–72.
10. Van den Heuvel MP, Sporns O. A cross-disorder connectome landscape of brain dysconnectivity. Nat Rev Neurosci. 2019;20(7):435–46.
11. Brettschneider J, Tredici KD, Lee VMY, Trojanowski JQ. Spreading of pathology in neurodegenerative diseases: a focus on human studies. Nat Rev Neurosci. 2015;16(2):109–20.
12. Agosta F, Spinelli EG, Basaia S, Cividini C, Falbo F, Pavone C, Riva N, Canu E, Castelnovo V, Magnani G. Functional connectivity from disease epicenters in frontotemporal dementia. Neurology. 2023;100(22):e2290–303.
13. Shafiei G, Markello RD, Makowski C, Talpalaru A, Kirschner M, Devenyi GA, Guma E, Hagmann P, Cashman NR, Lepage M. Spatial patterning of tissue volume loss in schizophrenia reflects brain network architecture. Biol Psychiatry. 2020;87(8):727–35.
14. Hansen JY, Shafiei G, Vogel JW, Smart K, Bearden CE, Hoogman M, Franke B, Van Rooij D, Buitelaar J, McDonald CR. Local molecular and global connectomic contributions to cross-disorder cortical abnormalities. Nat Commun. 2022;13(1):4682.
15. Li J, Long Z, Sheng W, Du L, Qiu J, Chen H, Liao W. Transcriptomic similarity informs neuromorphic deviations in depression biotypes. Biol Psychiatry. 2024;95(5):414–25.
16. Chopra S, Segal A, Oldham S, Holmes A, Sabaroedin K, Orchard ER, Francey SM, O'Donoghue B, Cropley V, Nelson B. Network-based spreading of gray matter changes across different stages of psychosis. JAMA Psychiat. 2023;80(12):1246–57.
17. Lytton WW. Computer modelling of epilepsy. Nat Rev Neurosci. 2008;9(8):626–37.
18. Vogel JW, Corriveau-Lecavalier N, Franzmeier N, Pereira JB, Brown JA, Maass A, Botha H, Seeley WW, Bassett DS, Jones DT. Connectome-based modelling of neurodegenerative diseases: towards precision medicine and mechanistic insight. Nat Rev Neurosci. 2023;24(10):620–39.
19. Seguin C, Sporns O, Zalesky A. Brain network communication: concepts, models and applications. Nat Rev Neurosci. 2023;24(9):557–74.
20. Liang X, Sun L, Liao X, Lei T, Xia M, Duan D, Zeng Z, Li Q, Xu Z, Men W. Structural connectome architecture shapes the maturation of cortical morphology from childhood to adolescence. Nat Commun. 2024;15(1):784.

21. Mišić B, Betzel RF, Nematzadeh A, Goni J, Griffa A, Hagmann P, Flammini A, Ahn Y-Y, Sporns O. Cooperative and competitive spreading dynamics on the human connectome. Neuron. 2015;86(6):1518–29.
22. Raj A, Kuceyeski A, Weiner M. A network diffusion model of disease progression in dementia. Neuron. 2012;73(6):1204–15.
23. Meier JM, van Der Burgh HK, Nitert AD, Bede P, de Lange SC, Hardiman O, van den Berg LH, van den Heuvel MP. Connectome-based propagation model in amyotrophic lateral sclerosis. Ann Neurol. 2020;87(5):725–38.
24. Weng Y, Larivière S, Caciagli L, Vos de Wael R, Rodríguez-Cruces R, Royer J, Xu Q, Bernasconi N, Bernasconi A, Thomas Yeo B. Macroscale and microcircuit dissociation of focal and generalized human epilepsies. Commun Biol. 2020;3(1):244.
25. Bernhardt BC, Rozen DA, Worsley KJ, Evans AC, Bernasconi N, Bernasconi A. Thalamo–cortical network pathology in idiopathic generalized epilepsy: insights from MRI-based morphometric correlation analysis. Neuroimage. 2009;46(2):373–81.
26. Novak JL, Miller PR, Markovic D, Meymandi SK, DeGiorgio CM. Risk assessment for sudden death in epilepsy: the SUDEP-7 inventory. Front Neurol. 2015;6:252.
27. Duma GM, Danieli A, Mento G, Vitale V, Opipari RS, Jirsa V, Bonanni P, Sorrentino P. Altered spreading of neuronal avalanches in temporal lobe epilepsy relates to cognitive performance: A resting-state hdEEG study. Epilepsia. 2023;64(5):1278–88.
28. Duma GM, Pellegrino G, Rabuffo G, Danieli A, Antoniazzi L, Vitale V, Scotto Opipari R, Bonanni P, Sorrentino P. Altered spread of waves of activities at large scale is influenced by cortical thickness organization in temporal lobe epilepsy: a magnetic resonance imaging–high-density electroencephalography study. Brain Commun. 2024;6(1):fcad348.
29. Baxendale S. Neuropsychological assessment in epilepsy. Pract Neurol. 2018;18(1):43–8.
30. Fischl B. FreeSurfer Neuroimage. 2012;62(2):774–81.
31. Kong R, Li J, Orban C, Sabuncu MR, Liu H, Schaefer A, Sun N, Zuo X-N, Holmes AJ, Eickhoff SB. Spatial topography of individual-specific cortical networks predicts human cognition, personality, and emotion. Cereb Cortex. 2019;29(6):2533–51.
32. Meng Y, Yang S, Chen H, Li J, Xu Q, Zhang Q, Lu G, Zhang Z, Liao W. Systematically disrupted functional gradient of the cortical connectome in generalized epilepsy: Initial discovery and independent sample replication. Neuroimage. 2021;230: 117831.
33. Yang S, Meng Y, Li J, Li B, Fan Y-S, Chen H, Liao W. The thalamic functional gradient and its relationship to structural basis and cognitive relevance. Neuroimage. 2020;218: 116960.
34. Van Essen DC, Smith SM, Barch DM, Behrens TE, Yacoub E, Ugurbil K, Consortium W-MH. The WU-Minn human connectome project: an overview. Neuroimage. 2013;80:62–79 https://db.humanconnectome.org/.
35. Tournier J-D, Smith R, Raffelt D, Tabbara R, Dhollander T, Pietsch M, Christiaens D, Jeurissen B, Yeh C-H, Connelly A. MRtrix3: A fast, flexible and open software framework for medical image processing and visualisation. Neuroimage. 2019;202: 116137.
36. Schaefer A, Kong R, Gordon EM, Laumann TO, Zuo X-N, Holmes AJ, Eickhoff SB, Yeo BT. Local-global parcellation of the human cerebral cortex from intrinsic functional connectivity MRI. Cereb Cortex. 2018;28(9):3095–114.
37. Betzel RF, Griffa A, Hagmann P, Mišić B. Distance-dependent consensus thresholds for generating group-representative structural brain networks. Netw Neurosci. 2019;3(2):475–96.
38. Brodoehl S, Gaser C, Dahnke R, Witte OW, Klingner CM. Surface-based analysis increases the specificity of cortical activation patterns and connectivity results. Sci Rep. 2020;10(1):5737.
39. Yeo BT, Krienen FM, Sepulcre J, Sabuncu MR, Lashkari D, Hollinshead M, Roffman JL, Smoller JW, Zöllei L, Polimeni JR. The organization of the human cerebral cortex estimated by intrinsic functional connectivity. J Neurophysiol. 2011;103(3):1125–65.
40. Mesulam MM. Principles of behavioral and cognitive neurology. Oxford University Press, 2000.
41. Alexander-Bloch AF, Shou H, Liu S, Satterthwaite TD, Glahn DC, Shinohara RT, Vandekar SN, Raznahan A. On testing for spatial correspondence between maps of human brain structure and function. Neuroimage. 2018;178:540–51.
42. Váša F, Seidlitz J, Romero-Garcia R, Whitaker KJ, Rosenthal G, Vértes PE, Shinn M, Alexander-Bloch A, Fonagy P, Dolan RJ. Adolescent tuning of association cortex in human structural brain networks. Cereb Cortex. 2018;28(1):281–94.
43. Burt JB, Demirtaş M, Eckner WJ, Navejar NM, Ji JL, Martin WJ, Bernacchia A, Anticevic A, Murray JD. Hierarchy of transcriptomic specialization across human cortex captured by structural neuroimaging topography. Nat Neurosci. 2018;21(9):1251–9.
44. Hawrylycz MJ, Lein ES, Bongaarts AL, Shen EH, Ng L, Miller JA, Van De Lagemaat LN, Smith KA, Ebbert A, Riley ZL. An anatomically comprehensive atlas of the adult human brain transcriptome. Nature. 2012;489(7416):391–9. https://human.brain-map.org/.
45. Markello RD, Arnatkeviciute A, Poline JB, Fulcher BD, Fornito A, Misic B. Standardizing workflows in imaging transcriptomics with the abagen toolbox. eLife. 2021;10:e72129.
46. Tilae C. Genome-wide mega-analysis identifies 16 loci and highlights diverse biological mechanisms in the common epilepsies. Nat Commun. 2018;9(1):5269.
47. Larivière S, Royer J, Rodríguez-Cruces R, Paquola C, Caligiuri ME, Gambardella A, Concha L, Keller SS, Cendes F, Yasuda CL. Structural network alterations in focal and generalized epilepsy assessed in a worldwide ENIGMA study follow axes of epilepsy risk gene expression. Nat Commun. 2022;13(1):4320.
48. Duma GM, Cuozzo S, Wilson L, Danieli A, Bonanni P, Pellegrino G. Excitation/Inhibition balance relates to cognitive function and gene expression in temporal lobe epilepsy: a high density EEG assessment with aperiodic exponent. Brain Commun. 2024;6(4):fcae231.
49. Goulas A, Changeux J-P, Wagstyl K, Amunts K, Palomero-Gallagher N, Hilgetag CC. The natural axis of transmitter receptor distribution in the human cerebral cortex. P Natl Acad Sci Usa. 2021;118(3): e2020574118.
50. Hansen JY, Shafiei G, Markello RD, Smart K, Cox SM, Nørgaard M, Beliveau V, Wu Y, Gallezot J-D, Aumont É. Mapping neurotransmitter systems to the structural and functional organization of the human neocortex. Nat Neurosci. 2022;25(11):1569–81 https://github.com/netneurolab/hansen_receptors.
51. Wagstyl K, Larocque S, Cucurull G, Lepage C, Cohen JP, Bludau S, Palomero-Gallagher N, Lewis LB, Funck T, Spitzer H. BigBrain 3D atlas of cortical layers: Cortical and laminar thickness gradients diverge in sensory and motor cortices. PLoS Biol. 2020;18(4): e3000678.
52. Paquola C, Vos De Wael R, Wagstyl K, Bethlehem RA, Hong SJ, Seidlitz J, Bullmore ET, Evans AC, Misic B, Margulies DS. Microstructural and functional gradients are increasingly dissociated in transmodal cortices. PLoS Biol. 2019;17(5):e3000284.
53. Amunts K, Lepage C, Borgeat L, Mohlberg H, Dickscheid T, Rousseau M-É, Bludau S, Bazin P-L, Lewis LB, Oros-Peusquens A-M. BigBrain: an ultrahigh-resolution 3D human brain model. Science. 2013;340(6139):1472–5 https://bigbrainwarp.readthedocs.io.
54. Paquola C, Royer J, Lewis LB, Lepage C, Glatard T, Wagstyl K, DeKraker J, Toussaint PJ, Valk SL, Collins L. The BigBrainWarp toolbox for integration of BigBrain 3D histology with multimodal neuroimaging. eLife. 2021;10:e70119.
55. Grömping U. Relative importance for linear regression in R: the package relaimpo. J Stat Softw. 2007;17:1–27.
56. Galovic M, van Dooren VQ, Postma TS, Vos SB, Caciagli L, Borzì G, Rosillo JC, Vuong KA, de Tisi J, Nachev P. Progressive cortical thinning in patients with focal epilepsy. JAMA Neurol. 2019;76(10):1230–9.
57. Xiao F, Caciagli L, Wandschneider B, Sone D, Young AL, Vos SB, Winston GP, Zhang Y, Liu W, An D. Identification of different MRI atrophy progression trajectories in epilepsy by subtype and stage inference. Brain. 2023;146(11):4702–16.
58. Pei H, Ma S, Yan W, Liu Z, Wang Y, Yang Z, Li Q, Yao D, Jiang S, Luo C. Functional and structural networks decoupling in generalized tonic–clonic seizures and its reorganization by drugs. Epilepsia Open. 2023;8(3):1038–48.
59. Jo HJ, Kenney-Jung DL, Balzekas I, Welker KM, Jones DT, Croarkin PE, Benarroch EE, Worrell GA. Relationship between seizure frequency and functional abnormalities in limbic network of medial temporal lobe epilepsy. Front Neurol. 2019;10:488.
60. Bharath R, Sinha S, Panda R, Raghavendra K, George L, Chaitanya G, Gupta A, Satishchandra P. Seizure frequency can alter brain connectivity: evidence from resting-state fMRI. Am J Neuroradiol. 2015;36(10):1890–8.

61. Rutherford S, Kia SM, Wolfers T, Fraza C, Zabihi M, Dinga R, Berthet P, Worker A, Verdi S, Ruhe HG. The normative modeling framework for computational psychiatry. Nat Protoc. 2022;17(7):1711–34.
62. Georgiadis F, Larivière S, Glahn D, Hong LE, Kochunov P, Mowry B, Loughland C, Pantelis C, Henskens FA, Green MJ. Connectome architecture shapes large-scale cortical alterations in schizophrenia: a worldwide ENIGMA study. Mol Psychiatry. 2024;29(6):1869–81.
63. Zhang Z, Liao W, Chen H, Mantini D, Ding J-R, Xu Q, Wang Z, Yuan C, Chen G, Jiao Q. Altered functional–structural coupling of large-scale brain networks in idiopathic generalized epilepsy. Brain. 2011;134(10):2912–28.
64. Li J, Keller SS, Seidlitz J, Chen H, Li B, Weng Y, Meng Y, Yang S, Xu Q, Zhang Q. Cortical morphometric vulnerability to generalised epilepsy reflects chromosome-and cell type-specific transcriptomic signatures. Neuropath Appl Neuro. 2023;49(1): e12857.
65. Betzel RF, Bassett DS. Specificity and robustness of long-distance connections in weighted, interareal connectomes. P Natl Acad Sci Usa. 2018;115(21):E4880–9.
66. Váša F, Mišić B. Null models in network neuroscience. Nat Rev Neurosci. 2022;23(8):493–504.
67. Jiang S, Huang H, Zhou J, Li H, Duan M, Yao D, Luo C. Progressive trajectories of schizophrenia across symptoms, genes, and the brain. Bmc Med. 2023;21(1):237.
68. Benuzzi F, Mirandola L, Pugnaghi M, Farinelli V, Tassinari CA, Capovilla G, Cantalupo G, Beccaria F, Nichelli P, Meletti S. Increased cortical BOLD signal anticipates generalized spike and wave discharges in adolescents and adults with idiopathic generalized epilepsies. Epilepsia. 2012;53(4):622–30.
69. Tangwiriyasakul C, Perani S, Abela E, Carmichael DW, Richardson MP. Sensorimotor network hypersynchrony as an endophenotype in families with genetic generalized epilepsy: a resting-state functional magnetic resonance imaging study. Epilepsia. 2019;60(3):e14–9.
70. Gotman J, Grova C, Bagshaw A, Kobayashi E, Aghakhani Y, Dubeau F. Generalized epileptic discharges show thalamocortical activation and suspension of the default state of the brain. P Natl Acad Sci Usa. 2005;102(42):15236–40.
71. Vollmar C, O'Muircheartaigh J, Barker GJ, Symms MR, Thompson P, Kumari V, Duncan JS, Janz D, Richardson MP, Koepp MJ. Motor system hyperconnectivity in juvenile myoclonic epilepsy: a cognitive functional magnetic resonance imaging study. Brain. 2011;134(6):1710–9.
72. Jiang S, Wang Y, Pei H, Li H, Chen J, Yao Y, Li Q, Yao D, Luo C. Brain activation and connection across resting and motor-task states in patients with generalized tonic–clonic seizures. CNS Neurosci Ther. 2024;30(4): e14672.
73. Yang S, Zhang Z, Chen H, Meng Y, Li J, Li Z, Xu Q, Zhang Q, Fan YS, Lu G. Temporal variability profiling of the default mode across epilepsy subtypes. Epilepsia. 2021;62(1):61–73.
74. Xia J, Liu C, Li J, Meng Y, Yang S, Chen H, Liao W. Decomposing cortical activity through neuronal tracing connectome-eigenmodes in marmosets. Nat Commun. 2024;15(1):2289.
75. Sainburg LE, Janson AP, Johnson GW, Jiang JW, Rogers BP, Chang C, Englot DJ, Morgan VL. Structural disconnection relates to functional changes after temporal lobe epilepsy surgery. Brain. 2023;146(9):3913–22.
76. Xie K, Royer J, Larivière S, Rodriguez-Cruces R, Frässle S, Cabalo DG, Ngo A, DeKraker J, Auer H, Tavakol S. Atypical connectome topography and signal flow in temporal lobe epilepsy. Prog Neurobiol. 2024;236:102604.
77. Kang J, Brajanovski N, Chan KT, Xuan J, Pearson RB, Sanij E. Ribosomal proteins and human diseases: molecular mechanisms and targeted therapy. Signal Transduction Targeted Ther. 2021;6(1):323.
78. Zhu L, Chen L, Xu P, Lu D, Dai S, Zhong L, Han Y, Zhang M, Xiao B, Chang L. Genetic and molecular basis of epilepsy-related cognitive dysfunction. Epilepsy Behav. 2020;104:106848.
79. Akyuz E, Polat AK, Eroglu E, Kullu I, Angelopoulou E, Paudel YN. Revisiting the role of neurotransmitters in epilepsy: An updated review. Life Sci. 2021;265:118826.
80. Royer J, Larivière S, Rodriguez-Cruces R, Cabalo DG, Tavakol S, Auer H, Ngo A, Park BY, Paquola C, Smallwood J. Cortical microstructural gradients capture memory network reorganization in temporal lobe epilepsy. Brain. 2023;146(9):3923–37.
81. Li J, Seidlitz J, Suckling J, Fan F, Ji G-J, Meng Y, Yang S, Wang K, Qiu J, Chen H. Cortical structural differences in major depressive disorder correlate with cell type-specific transcriptional signatures. Nat Commun. 2021;12(1):1647.
82. Ji G-J, Zhang Z, Xu Q, Zang Y-F, Liao W, Lu G. Generalized tonic-clonic seizures: aberrant interhemispheric functional and anatomical connectivity. Radiology. 2014;271(3):839–47.
83. Gloor P, Guberman AH. The temporal lobe & limbic system. Can Med Assoc J. 1997;157(11):1597.
84. Pitcher D, Ungerleider LG. Evidence for a third visual pathway specialized for social perception. Trends Cognit Sci. 2021;25(2):100–10.
85. Rodriguez-Cruces R, Royer J, Larivière S, Bassett DS, Caciagli L, Bernhardt BC. Multimodal connectome biomarkers of cognitive and affective dysfunction in the common epilepsies. Netw Neurosci. 2022;6(2):320–38.
86. Li R, Liao W, Li Y, Yu Y, Zhang Z, Lu G, Chen H. Disrupted structural and functional rich club organization of the brain connectome in patients with generalized tonic-clonic seizure. Hum Brain Mapp. 2016;37(12):4487–99.
87. Markello RD, Hansen JY, Liu Z-Q, Bazinet V, Shafiei G, Suárez LE, Blostein N, Seidlitz J, Baillet S, Satterthwaite TD. Neuromaps: structural and functional interpretation of brain maps. Nat Methods. 2022;19(11):1472–9.

Publisher's Note